Design of a Carbon-Fiber-Reinforced Wing for the Alpha-Jet Major Panel Tests

D. Rose* and E. Henze*
Dornier GmbH, Friedrichshafen, Federal Republic of Germany
and
D. Wurzel* and H. Schelling*
Deutsche Forschungs- und Versuchsanstalt für Luft- und Raumfahrt e.V.
Stuttgart, Federal Republic of Germany

Dornier Company is presently developing a carbon-fiber-reinforced plastic (CFRP) wing for its ground support aircraft Alpha-Jet. It incorporates CFRP-skins and spars, with the skins being integrally stiffened with stringer blades and manufactured in a one-shot autoclave process. Skin design and manufacturing technology were of great concern due to in-plane and transverse loads and instability, on one hand, and, the demand for reproducibility, on the other. To show the efficiency of the design and manufacturing approaches, two different components of the tank end area were tested and compared at DFVLR, the German Aerospace Research Establishment. Test results showed good agreement with the theoretical data which permitted the go-ahead in the development. This report describes the design and manufacturing philosophy and the experimental setup, and compares the test results to the expected values.

Introduction

AT Dornier Company, composite technology was developed and tested primarily on graphite/epoxy components for the Alpha-Jet ground support aircraft. The end of the development chain of plane load-bearing structures—air brake, vertical tail rudder, horizontal stabilizer—is the pressurized wing (Fig. 1). At present the static fracture test wing is being manufactured.

After comparative studies of various basic configurations, the multirib version with stringer stiffened skins was preferred over the multispar version. All movable parts, leading edges, and the wing-tip formers were taken from the series production. The ribs were made of metal, and the skins and spars were manufactured in one shot from carbon fiber prepreg (Fig. 2).

The design and manufacturing of skins adaptable to quantity production were considered the main development risks. In this article the testing of the primary components to verify the design and manufacturing philosophy will be described. The tests were prepared and performed by DFVLR, the German Aerospace Research Establishment, and the panels were provided by Dornier.

Skin Design and Manufacturing

Structural loading results from air and mass loads due to required flight maneuvers and pressurization of the tank. Stress resultants due to maneuver loads were determined by finite element analysis with Dornier's COSA program system. Bending moments resulting from tank pressure were calculated by means of a beam-grid-model for the skin strips and the perpendicular stringer sections.

The environmental effects on mechanical property values were taken into account by introducing envelope curves for the 175°C systems, T300/Code 69 and Fiberite 1076 which are valid for 85% relative humidity and operating temperatures between −55 and 70°C.

The quadratic failure criterion applied allows for unforeseeable holes and damages by means of a stress concentration factor $1.7 < \alpha < 2$. Stresses resulting from the superposition of maneuver and tank pressure loads were determined by 2nd order theory. This led to the design of a skin stiffened with nonparallel blade stringers. The stringer spacing changes at the tank end rib. The laminates are predominantly quasi-isotropic with fiber orientations in the 0, ±45, and 90 deg directions. The characteristic construction of the panels is determined by joining *u*-shaped sections on a base laminate with the junction planes forming symmetry planes. Local reinforcements consist of symmetric laminates with 2 mm single ply steps which are placed in the symmetry planes (Fig. 3). Relative stringer dimensions are

$$s_{\text{blade}} = s_{\text{skin}} \quad \text{and} \quad 2\,h_{\text{blade}} = b_{\text{stringer}}$$

The skin thickness varies from 8 to 2 mm, and stringer spacing varies from 80 to 40 mm.

The stringer stiffened skins are manufactured in one shot in an autoclave. Pressure pieces made of thermal expansion rubber and a semirigid reinforced rubber blanket are employed to mold the skin (Fig. 3). These tools are also used for transforming the flat stringer laminates into *u*-shaped profiles.

Development Risks and Necessary Tests

The main development risks found, respectively, were in the design, due to the combined membrane and plate stresses and the stability analysis; and in the development of a reproducible manufacturing process for parts of acceptable quality. To cover these risks and to verify the design and manufacturing approaches, different wing panel sections were tested.

Basic tests included the tank end area with membrane and tank pressure loads and their combination (Fig. 4). The first approach was made with test panel type-I. Laminate thicknesses, stringer height, and stringer spacing of panel I correspond to the lower wing skin section between ribs 8 and 9.

Received April 11, 1985; presented as Paper 85-0725 at the AIAA/ASCE/AHS Structures, Structural Dynamics and Materials Conference, Orlando, FL, April 15-17, 1985; revision received Dec. 18, 1986.

*Engineer.

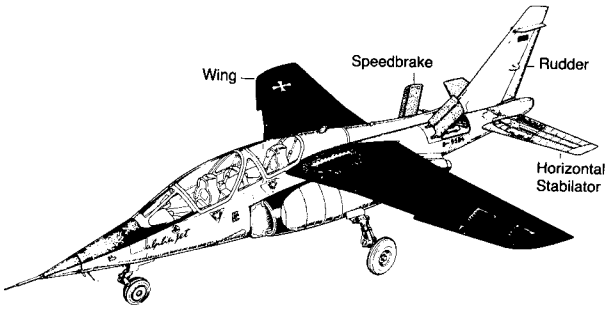

Fig. 1 Alpha-Jet: flying testbed for CFRP components.

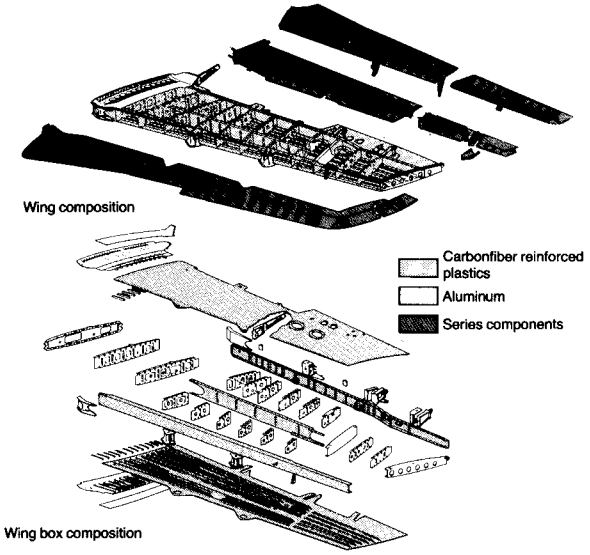

Fig. 2 CFRP wing for the flying testbed Alpha-Jet.

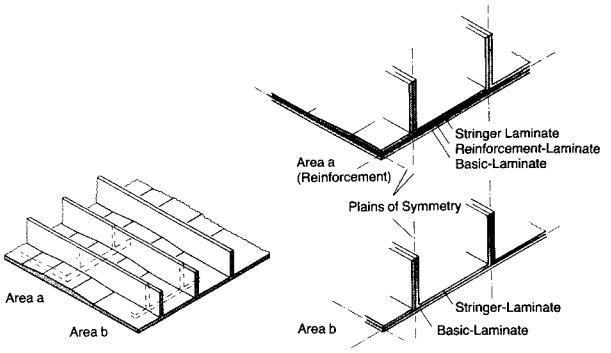

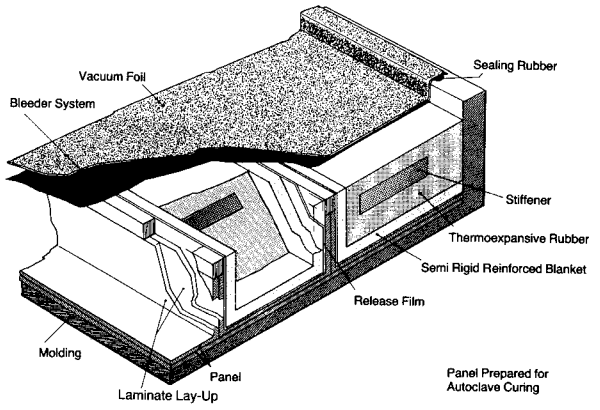

Fig. 3 Integrally stiffened CFRP-panel details of lay-up, manufacturing.

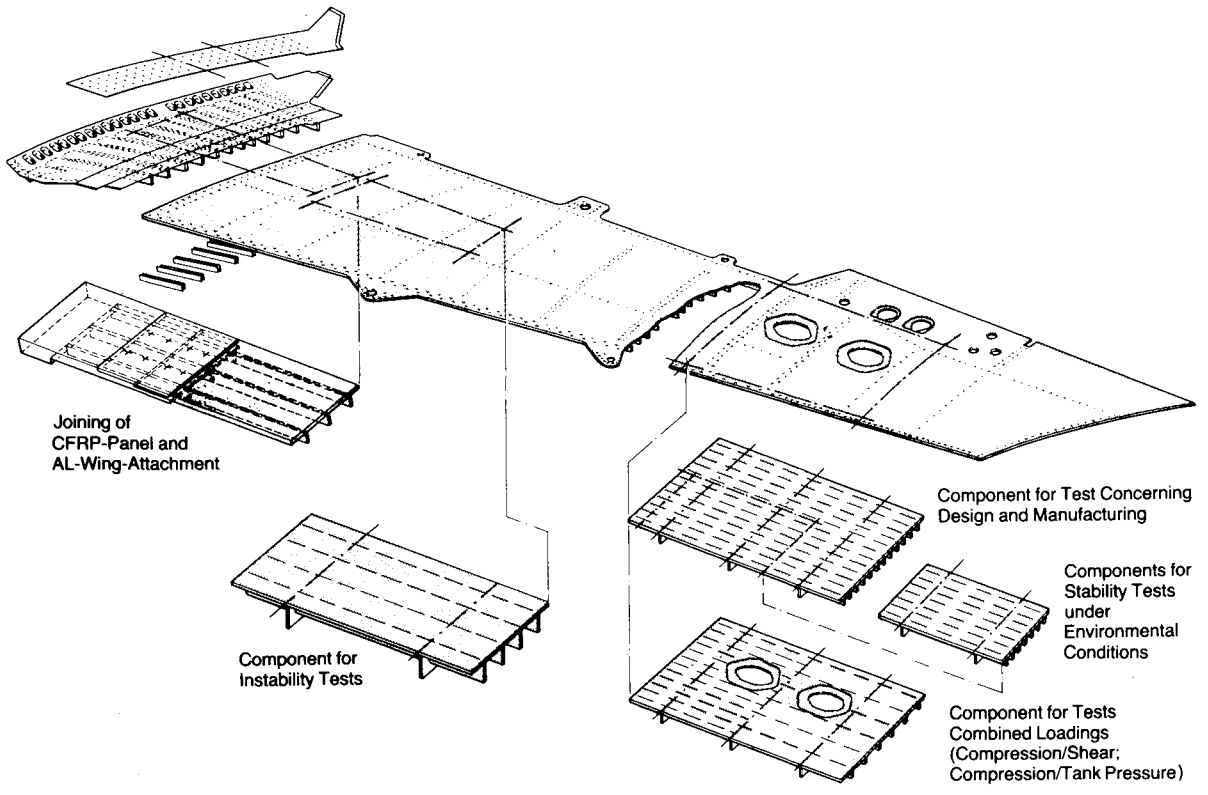

Fig. 4 CFRP-panel and its test components.

Table 1 Tests performed and results

Loading	n_y, N/mm	N_y, kN	P_i, bar	Load factor j section between ribs 8-9	9-10
Panel 1					
1) Tension	362.5	235.9	—	1.45	
2) Compression	362.5	−236.3	—	1.45	
3) Tank pressure + roll loads	—	—	2.63	(1.43)	
4) Tension + tank pressure	357.5	233.6	0.86	1.43	
5) Compression + tank pressure[a]	625.0	−408.2	0.85	2.50	
6) ____	—	—	—	—	
Panel 2					
1) Tension	285.0	186.3	—	1.25	1.43
2) Compression	222.5	−144.5	—	0.89	1.41
3) Tank pressure + roll loads	—	—	2.67	(1.45)	—
4) Tension + tank pressure	322.5	210.9	0.88	1.41	1.62
5) Compression + tank pressure+	225.0	−146.5	0.90	0.90	1.43
6) Tension + tank pressure[a]	682.5	445.3	0.86	2.99	3.43

[a]Tests to failure.

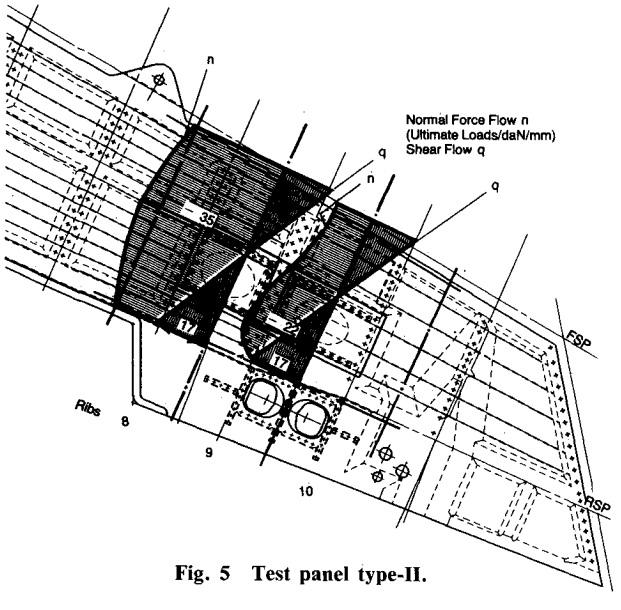

Fig. 5 Test panel type-II.

Due to the lack of curvature and the overall constant stringer spacing, Fig. 4 represents a simplistic model but presents an easy access for calculations. Panel type-II (Fig. 5) is a less simplified model of the upper wing skin between ribs 8 and 10, incorporating all characteristic design details though still flat and with parallel stringer spacing.

Stringer spacing was 40 mm between ribs 8 and 9, and 80 mm between ribs 9 and 10. With panel II, the effects of the cutouts and the efficiency of the connected covers were also to be tested. The covers with the cutouts correspond completely to those in the original wing. Between ribs 8 and 9 in the tank area, the unstiffened cover has a constant thickness of 5 mm.

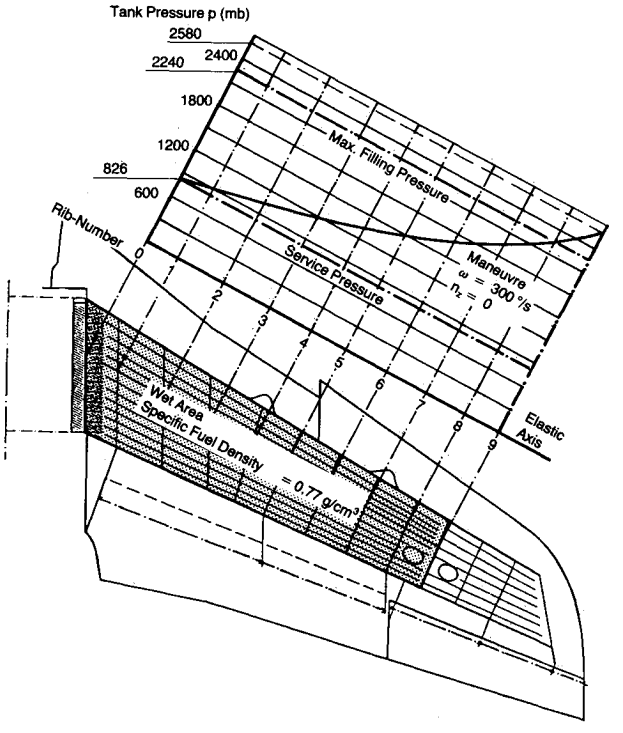

Fig. 6 Tank pressure distribution.

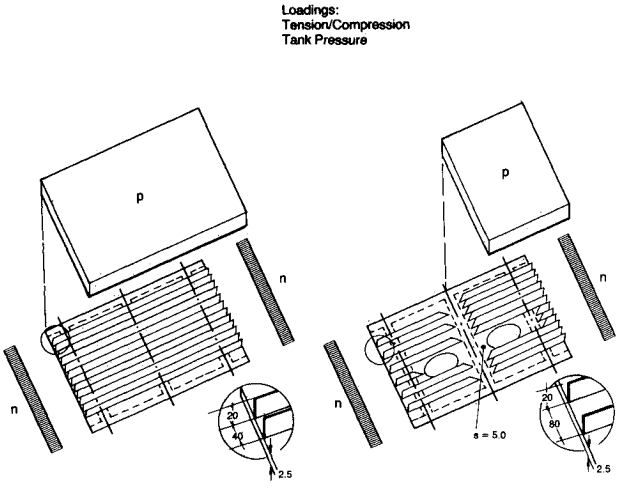

Fig. 7 Test panels: Location and loadings.

Between ribs 9 and 10, the cover is 2.5 mm thick and stiffened with an aluminum L-section. The material used for both panels is T300/Code 69. Each panel measures 1076×700 mm in size. Both panels were subjected to tension and compression and simulated tank pressure (Fig. 6).

All in-plane and transverse loads were applied separately and in combination. Panel loads were increased up to the ultimate loads in the corresponding skin area for all reasonable load configurations. Testing was concluded with fracture tests under the most critical combinations. Load levels were taken from the calculated maximum compression stress resultants at fracture in the upper or lower wing skins (Fig. 7). The aim was to measure the load bearing capability of the CFRP panels and register strains, strain distributions, and stress concentrations and compare them with analytically obtained values.

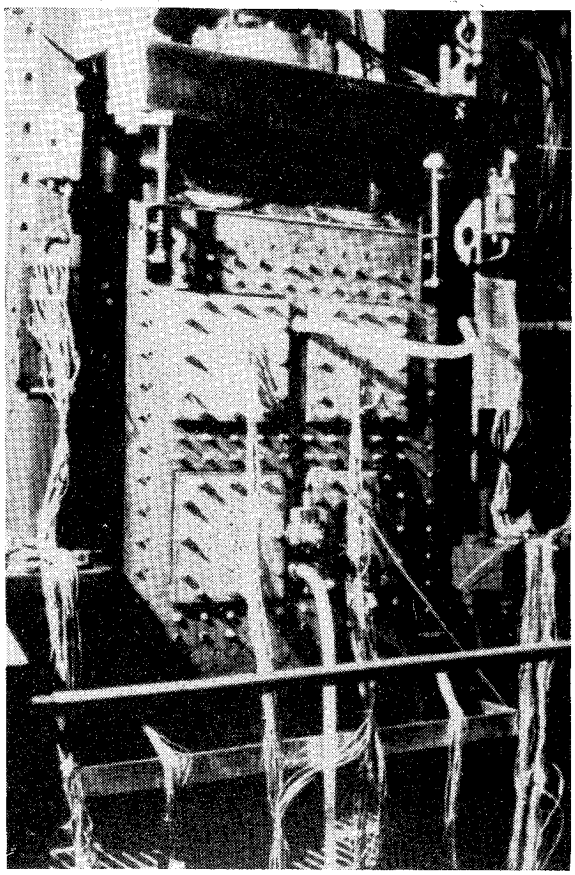

Fig. 8 Pressure casing in the loading frame.

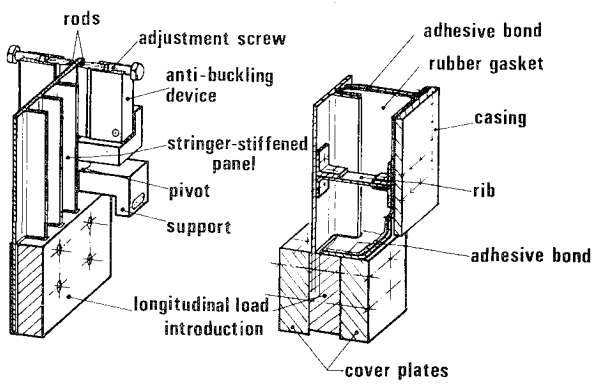

Fig. 9 Panel load application.

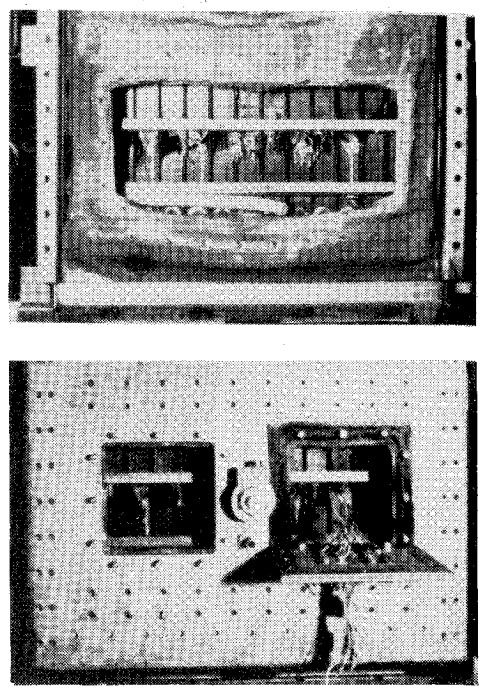

Fig. 10 Pressure casing with rubber gasket (top) and access doors (bottom).

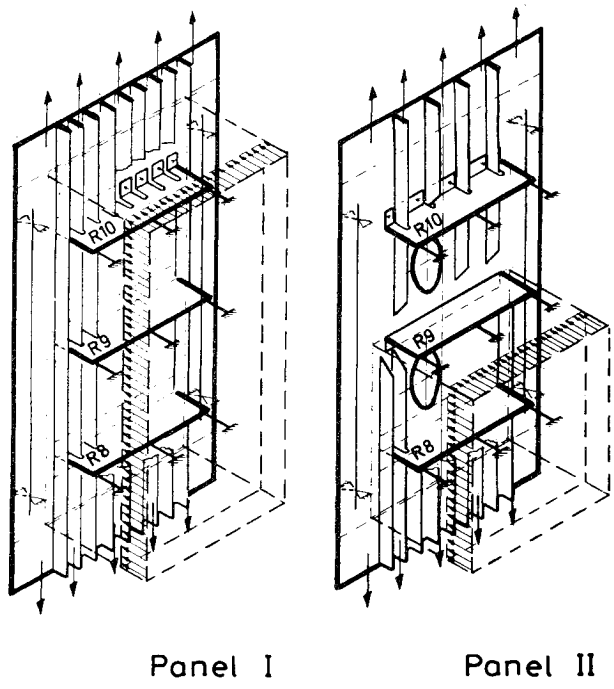

Fig. 11 In-plane loadings and pressurized areas.

Experimental Setup

The experimental setup included a loading frame with a 1000 kN electronically monitored hydraulic cylinder for tension and compression loading. To simulate the tank pressure, a casing was attached to the panel in the frame (Fig. 8). Thus a closed chamber was formed which could be pressurized. Special care was taken in the overall design to prevent any mutual interference or constraints between the loading frame and pressure chamber. Care was also taken to insure accurate in-plane and transverse loading of the panel and to correctly transfer pressure loads to the panel from the upper casing wall representing the tank end rib.

To insure an even introduction of in-plane loads over the full width of the panel, slotted aluminum bars were bonded to the stringer side panel ends. CFRP straps were bonded to the flat panel ends. This load introduction could cope well with panel fabrication tolerances and avoided stress peaks and transverse constraints. To connect the panel to the loading frame, the ends were bolted to steel coverplates. To simulate the stabilizing effect of the wing box spars during compression, antibuckling devices were installed at the free panel edges. These were pin jointed in the supports. Teflon rods were inserted between the devices and the panel to insure a linear support and to minimize friction (Fig. 9), and the antibuckling devices were suspended on springs to compensate for their weight.

Tank pressure was simulated by pressurized water for safety reasons. As in reality, the pressure loads had to be

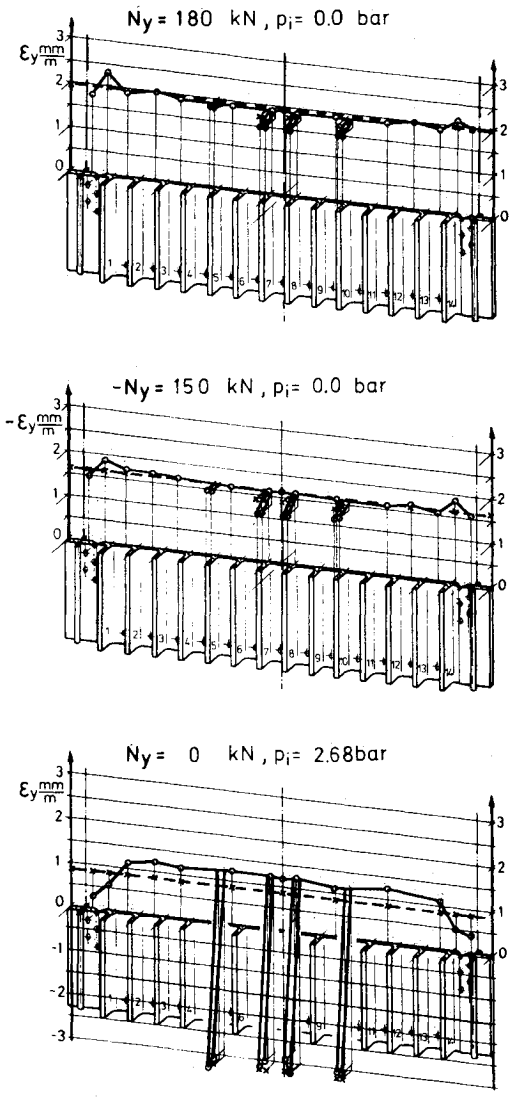

Fig. 12 Selected longitudinal strain distributions in skin and stringers. Panel I: tension (top), compression (center), and tank pressure (bottom).

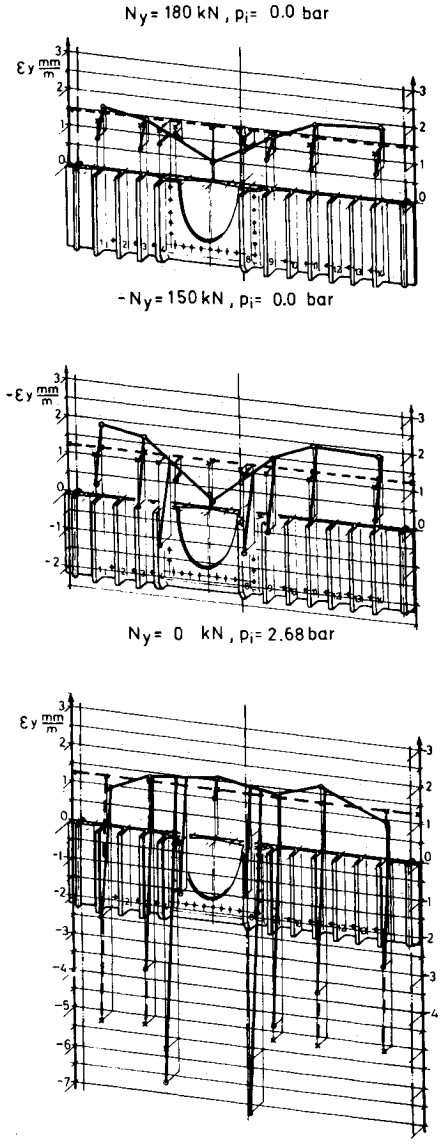

Fig. 13 Selected strain distributions in panel II: tension (top), compression (center), and tank pressure (bottom).

taken up by the ribs, which were connected to the bottom of the casing. Otherwise, the casing was completely decoupled from the panel, and therefore, no constraints could result. To seal the casing against the panel, a highly elastic rubber gasket was bonded in place. The sides of the casing were supported by cross members. At the bottom of the casing access doors were provided for assembly and inspection purposes. The doors allowed passage of strain gage cables (Fig. 10). Again, the casing was suspended on springs to make up for the additional weight. Pressure was allowed to act on the complete inner side of panel I but only on half of panel II, taking into account the end of the tank area (Fig. 11).

Strain Gage Arrangements and Data Acquisition

Up to 104 strain gages—single gages, 0/90-rosettes, and 0/45/90-rosettes—were bonded to different parts of each panel. Thus, normal stress resultants caused by longitudinal load, bending and transverse loads due to tank pressure, and stress concentrations, e.g., around rivet holes, as well as buckling of skin and stringers, could be checked. The gages were protected with a thin silicon layer against humidity and mechanical damage. Furthermore, longitudinal load, hydraulic ram displacement, and tank pressure were registered. Data accumulation was done at 5 ms intervals, a complete cycle was followed by a 2 s interval.

The tests were load-controlled. Loads were linearly increased; maximum loads were reached after 1 min and had to be sustained for at least 3 s. Fracture loads were also reached after about 1 min.

All recorded data were later evaluated and printed in diagrams to show the overall panel performance under load. By means of the resulting stress-strain-diagrams, stress resultants, stability limits, and stress concentrations were found and could be compared with calculated values.

During some tests, one panel was equipped with four acoustic emission sensors, one at each corner. There was a correlation between acoustic events and strain gage registered jogs. The number of events was clearly influenced by the preceding tests.

Test Results

All loading tests caused a rather uniform strain distribution over the panel width between ribs 8 and 9 of panel I

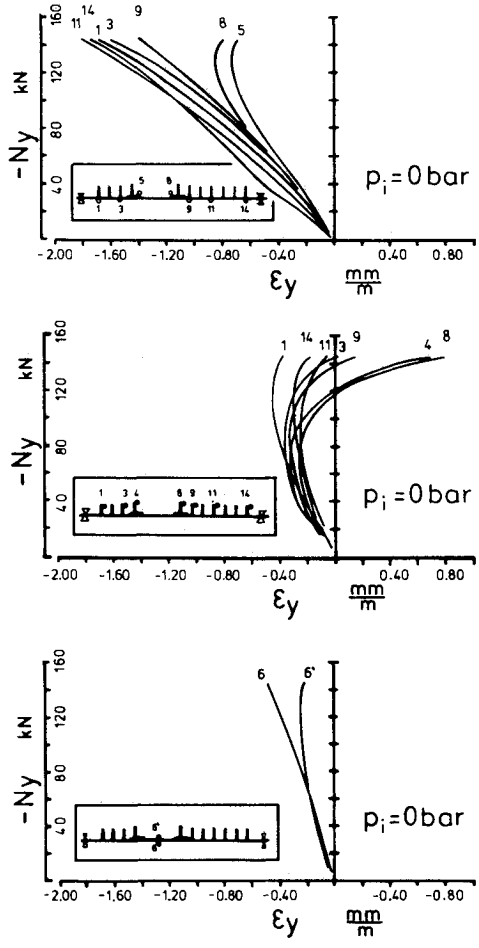

Fig. 14 Longitudinal strains in panel II. Insert shows cross section with strain gage positions: skin strains (top), stringer strains (center), and cover strains (bottom).

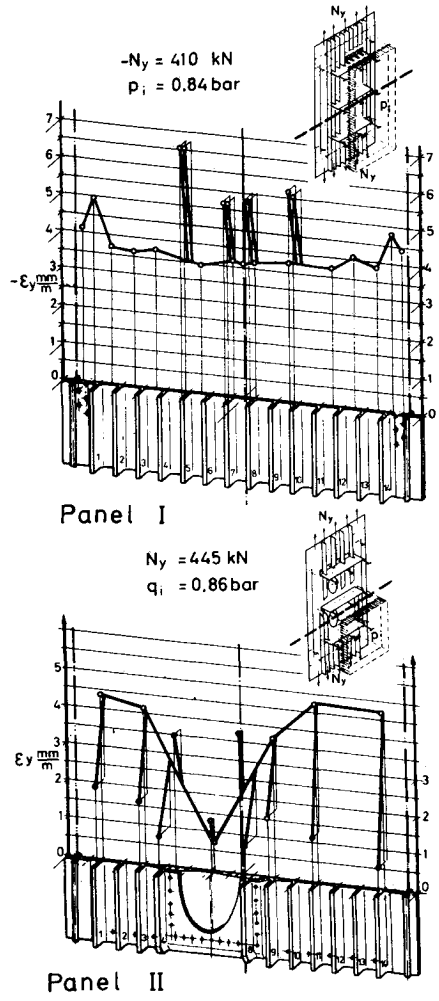

Fig. 15 Strain distribution in skins and stringers at failure load. Panel I: compression + tank pressure (top); panel II: tension and tank pressure (bottom); position of strain gages is along dotted line in inserts.

(Fig. 12). The slightly increased strains at the panel edges during longitudinal loading were caused by the rows of rivets. With tank pressure only, stresses decreased at the edges due to the antibuckling devices. It is evident that resulting stresses from combined loads can be obtained by superposing stresses from single loads as long as no deflections occur. Solid lines represent experimental results and dotted lines give theoretical values. Agreement between analytical and experimental results is rather good.

As for panel II (Fig. 13), pure tension caused a relatively uniform strain distribution up to the edges of the cutouts in the wet area betwen ribs 8 and 9. The load carrying capability of the cover was less than expected. Buckling under compression started at rather low load levels (Fig. 14). At $Ny = 70$ kN, the load-strain curves show deviations from linearity or even reversing strains. Especially those strain gages at or near the cover edges as well as at the cover center indicated a marked buckling. The stiffened cover between ribs 9 and 10 exhibited a better load carrying capability during longitudinal loading. Under compression, the covers carried about 10% less loads than under tension. Again, the mean analytical and experimental loads agreed well. The average strain levels in panel II were about 25% less than in panel I, since panel II had a higher cross-sectional area due to reinforcements around the cutouts. The cutouts also led to bending stresses under longitudinal loads. Both panels exhibited bending strains under maximum tank pressure; however, the cut out caused neighboring stringer strains to be about twice as high.

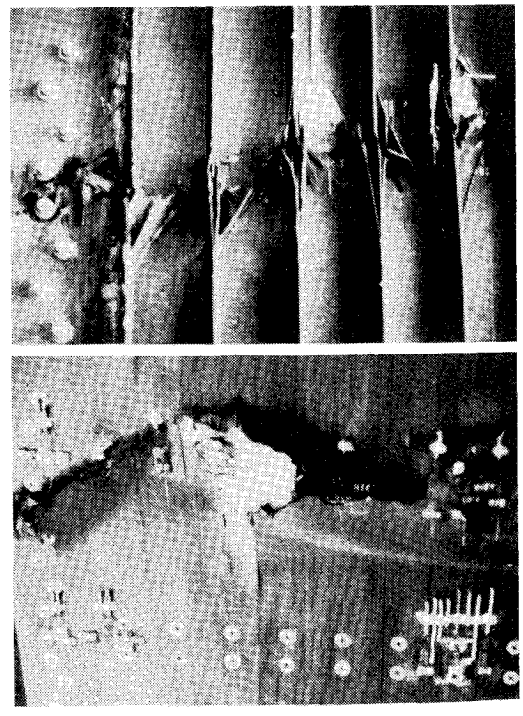

Fig. 16 Typical damages (panel I).

During the fracture test panel I was subjected to compression and tank pressure loads. Stress-strain diagrams indicated a linear behavior up to $j=2.41$. This means the stability limit was very close to the panel failure at $j=2.5$ ($-Ny=410$, $pi=0{,}84$ bar). Failure most probably initiated at stringer No. 5, which exhibited the highest strains (Fig. 15). The failure zone was in the middle between ribs 8 and 9 and was characterized by buckling damages and delaminations as well as spalling of the stringers (Fig. 16).

The differences between the predicted failure load $Ny=340$ kN and the actual failure load $Ny=445$ kN can be explained first by the very conservative design allowables ($\sigma_x=1200$ N/mm^2, $\sigma_y=\tau_{xy}=70$ N/mm^2) and by the underestimation of the loadcarrying capability of the access door in the section between ribs 9 and 10. Failure in both panels occurred in a sudden burst without visible deformations. Delaminations and stringer spalling occurred especially in the symmetry planes, e.g., the junction planes. All tests and load factors are presented in Table 1.

Conclusion and Outlook

The good agreement between calculated and test values up to failure loads confirms the efficiency of both the analytical approach and the manufacturing method. By taking into account the real geometric dimensions the results obtained can be made to apply to the original skin structure. Thus the technical risks are thought to be covered. Based on these results production of the complete wing was begun. The work was concluded by the end of 1985. The static test is planned for the second quarter of 1986.

Acknowledgment

The contributions of Mr. Harald Kraft of the DFVLR testing department to this project are gratefully acknowledged.